Electronic Supplementary Material (ESI) for Energy & Environmental Science.

Supporting Information

In-situ interface engineering of highly nitrogen-rich triazine-based covalent organic frameworks for ultra-stable, dendrite-free lithium-metal anode

Liguo Yue, Xinying Wang, Li Chen, Dijun Shen, Zhuhang Shao, Hao Wu, Shengfu Xiao, Weiquan Liang, Yaojiang Yu, Yunyong Li*

School of Materials and Energy, Guangdong University of Technology, No. 100 Waihuan Xi Road, Guangzhou Higher Education Mega Centre, Guangzhou, 510006, PR China

Corresponding author: *E-mail: yyli@gdut.edu.cn (Y.Y. Li). Tel: (+8620)-39322570, Fax: (+8620)-39322570. ORCID: https://orcid.org/0000-0002-8005-8207

Experiment Detail

1. Materials preparations

1.1 Materials

Melamine (MA, 98.0wt %), cyanuric acid (CA, 99.0wt %), (3-aminopropyl)triethoxysilane ($C_9H_{23}NO_3Si$, 98%) were purchased from Aladdin Reagent Inc. Dimethyl sulfoxide（DMSO, 99.9%）and ethanol were purchased from Tianjin Zhiyuan Chemical Reagent Co., Ltd. The electrolyte, 1,3-dioxolane, 1,2-dimethoxyethane and 1,3-dioxolane/1,2-dimethoxyethane (DOL/DME, v/v=1:1) were were purchased from DoDoChem Suzhou. All reagents in the experiment were chromatographically pure/analytical grade, which were employed without further purification.

1.2 Preparation of COF

In a typical synthesis, 1.0 mmol of Melamine (MA) and cyanuric acid (CA) were dispersed in 8 and 4 mL of dimethyl sulfoxide, respectively. Then, two mixtures sonicated for a few minutes to obtain an evenly mixed solution, and the two clear solutions were mixed together and placed on a stirrer for 12 h at room temperature. After the reaction was completed, it was left to stand for aging treatment. The white precipitate was washed with dimethyl sulfoxide and ethanol several times, and dried in an oven at 60 °C for overnight.

1.3 *In-situ* preparation of COF film on lithium foil

Firstly, MA and CA of the same molar mass were dissolved in 40 and 20 mL of DMSO solution, respectively. And then, 5 μL as-prepared amination reagent ((3-aminopropyl)

triethoxysilane, $NH_2(CH_2)_3Si(OC_2H_5)_3$) was dropped on the surface of the polished Li foil (the surface oxides of Li foil was removed by a drawknife) and coated evenly, and then, they were dried on a heated plate at 80 °C for 24 h (here, the purpose of amination on the polished Li is to construct the closure structure ($-NH_2$) for uniform polymerization of COF. And the construction of silicified organic interface can facilitate the uniform polymerization of COF. Meanwhile, the silicified hydrophobic organic interface layer can obstruct the reaction of water with Li metal in subsequent reactions (see **Figure S7**)). After the solvent on the surface of the lithium foil was completely evaporated, 10 μL CA solution was dropped onto Li foil. And then, MA solution was also dropped onto Li foil and reacted with CA at 40 °C for 12 h. Finally, the as-obtained COF modified Li foil (COF@Li) was washed by using DMSO and a volatile solvent tetrahydrofuran (THF) for several times. Subsequently, it was dried under the glove box at 40 °C for 12 h until the solvent is completely evaporated. Likewise, a COF modified Cu (COF@Cu) sample was also fabricated with the same conditions as COF@Li in addition to using Cu foil instead of Li foil. All above operations were in an Ar-filled the glove box (O_2<0.01 ppm; H_2O<0.01 ppm).

2. Materials characterizations

The morphologies and microstructures of samples characterized by field emission Scanning Electron Microscope (SEM, JEM-6700F, Hitachi-SU8010, Japan) equipped electron dispersive X-ray spectroscopy (EDS) mappings under an accelerating voltage of 200 kV. The X-ray diffraction (XRD) patterns were observed on a Rigaku Dmaxrc diffractometer XRD-6100 spectrometer with Cu Kα radiation λ=1.504 Å operated at 40

kV voltage and 40 mA current and the diffraction angle was stepped between 5-80 ° with at a scan rate of $8°\cdot min^{-1}$. The X-ray photoelectron spectroscopy (XPS, Escalab 250Xi, Thermo Fisher, USA) was recorded to measure the chemical state, chemical composition and molecular structure of the material with monochromatic 150 W Al-K(α) radiation at the working voltage of 15 kV and current of 15 mA. The COF was identified by Fourier Transform Infrared spectrograph (FTIR, NICOLET 6700) spectra. The specific surface area (SSA) and pore size distribution (PSD) were tested using a Brunauer-Emmett-Teller (BET, ASAP 2460 surface area analyzer Micromeritics Co., Norcross, GA). The contact angles were tested using a SL200 KB apparatus at room temperature. *In-situ* optical microscopy measurement (LW750LJT, CEWEI, Beijing) was observed the dendrite growth process by an *in-situ* cell (LIB-MS, Beijing Scistar Technology Co. Ltd) equipped with quartz window on top. Atomic force microscopy (AFM) measurement was conducted on Bruker Dimension icon to Young's modulus (Cantilever: 200N/m). Time-of-flight secondary ion mass spectrometry (ToF-SIMS) was carried out with a 2 keV Cs^+ beam in the negative mode to sputter the anodes and produce secondary ions (or molecular fragments). A pulse (20 ns) 30 keV Bi^+ beam in high-current mode was used for depth profiling with an area of 80 × 80 μm^2.

3. Electrochemical measurements

The symmetric cells of Li ‖ Li and COF@Li ‖ COF@Li were assembled with CR2032 coin, a commercial Clegard 2400 polypropylene film as a separator, and 40 μL of 1.0 M LiTFSI dissolved in 1,3-dioxolane (DOL) and 1,2-dimethoxyethane (DME) (v/v = 1:1) with 1 wt % $LiNO_3$ as electrolyte. The Li | Cu half cells are only replaced the

electrode on the side of the symmetrical cell described above with copper foil. The prepared copper foil was firstly punched into 12 mm diameter discs, then placed in a beaker and washed with alcohol ultrasonically (remove impurities left over from industrial production), and dried for later use. The fresh Li | Cu half cells were activated for 10 cycles at 50 μA cm^{-2} between 0.1 and 1.0 V to purify the surface and stabilize the SEI. Then, fixed amount of Li (1.0, 2.0, 5.0 and 8.0 mAh cm^{-2}) was deposited on copper foil current collector and stripped away Li until the charge voltage reaching 1.0 V at different current densities in each cycles. To fabricated $LiFePO_4$ cathode, the mixture consists of $LiFePO_4$, carbon nanotubes (CNTs) and polyvinylidene difluoride (PVDF) (w/w = 7:2:1) were grind for 0.5 h before adding into N-methyl-2-pyrrolidone (NMP), and the mass loading of LFP is 5~7 mg cm^{-2} for route test. The full cell was tested using ether and esters electrolytes, i.e. 1.0 M LiTFSI dissolved in DOL/DME (v/v = 1:1) with 2 wt % $LiNO_3$. These full cells were employed to acquire cycling stability and rate performance at a LAND-CT2001A battery test system (1.0 C = 170 mAh g^{-1}). Cyclic voltammetry (CV) and electrochemical impedance spectroscopy (EIS) were recorded on an electrochemical workstation (CHI660E, Shanghai Chenhua).

The thermal activation energy was calculated from an Arrhenius Eq.S1 and derived from an Arrhenius type relationship Eq. S2.

$$k = Ae^{-E_a/RT} \quad \textbf{(S1)}$$

$$lnk = -\frac{E_a}{RT} + lnA \quad \textbf{(S2)}$$

where *k*, *A*, *Ea*, *R*, and *T* corresponding to the rate of a reaction, Frequency factor, activation energy of the reaction, gas constant and temperature (range from 303 to 323

K), respectively.

The time dependence of current flowing through the COF@Li||COF@Li symmetric cell with a voltage of 20 mV (ΔV) applied, and the interfacial resistance of the cell before (R_0) and after (Rs) polarization were measured by EIS (estimated by semicircle diamters from impedance spectra), the t_{Li+} was calculated based on **Eq**. **S3**:

$$t_{Li+} = \frac{I_s(\Delta V - I_0 R_0)}{I_0(\Delta V - I_s R_s)} \quad \text{(S3)}$$

where I_0 and R_0 is the initial current value and resistance, I_s and R_s is the stable current value and resistance after polarization.

The D_{Li+} can be calculated from slopes of the line in the low-frequency region, and Li^+ diffusion coefficients were calculated by using the following **Eq**. **S4** and **S5**.

$$Z_{re} = R_{ct} + R_s + \sigma\omega^{-1/2} \quad \text{(S4)}$$

$$D_{Li+} = \frac{R^2T^2}{2A^2n^4F^4C_{Li}^2\sigma^2} \quad \text{(S5)}$$

where R, A, T, F, C, n, ω and σ corresponding to the gas constant, surface area of the electrode, temperature, Faraday constant, concentration of Li^+, number of electrons, frequency and Warburg factor, respectively. The Warburg factor is displayed from Z' *vs*. $\omega^{-1/2}$ diagram

4. Theoretical Calculation

The DFT calculations were performed by Vienna Ab initio Simulation Package (VASP) [S1], and the projector augmented wave (PAW) pseudopotentials [S2] were used to describe the electron-ion interaction, the exchange-functional was treated using the

generalized gradient approximation (GGA) of Perdew-Burke-Ernzerhof (PBE) [S3] functional. After the accuracy test, the 500eV energy cutoff for the plane wave basis expansion was setted, and 2×2×1 grids in *k*-point were sampled. Then the force on each atom less than 0.03 eV/Å was setted for convergence criterion of geometry relaxation. In order to avoid the interaction between periodic structures, a 15 Å vacuum was added along the *z* direction, and the DFT-D3 method was employed to consider the van der Waals interaction [S4]. The climbing-image nudged elastic band (CI-NEB) method [S5] was used to calculate the energy barrier for Li diffusion path. The adsorption energy of Li was calculated according to

$$E_{ads} = E_{total} - E_{C_2N_3} - E_{Li}$$

where E_{total} is the total energy of the Li adsorbed systems, $E_{C_2N_3}$ and E_{Li} are the energies of the substrate and the isolated Li atom, respectively. The Gibbs free energy of adsorption behavior in C_2N_3 system was calculated by the expression:

$$\Delta G_{(n+1)Li} = G_{(n+1)Li} - G_{nLi} - G_{Li}$$

Where G_{nLi} is the Gibbs free energy of C_3N_2 system with nLi adsorption, $G_{(n+1)Li}$ is the final Gibbs free energy of (n+1) Li insert into the C_3N_2 system, and G_{Li} can be replaced by the single Li energy in the BCC Li bulk.

5. Figures

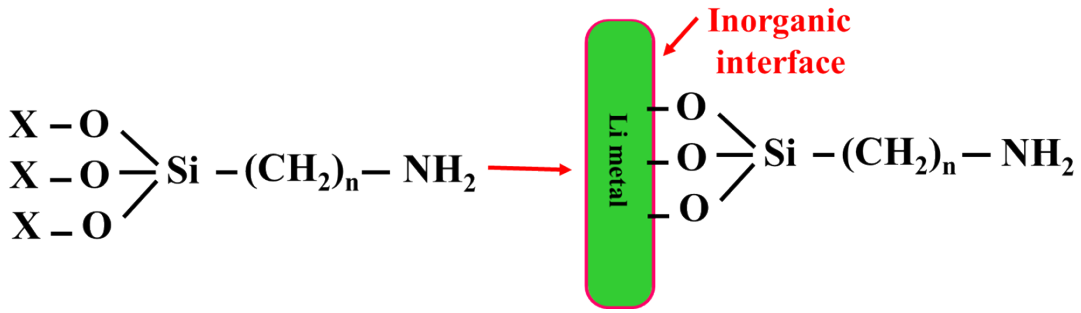

Figure S1 Mechanism of silanization on Li metal surface.

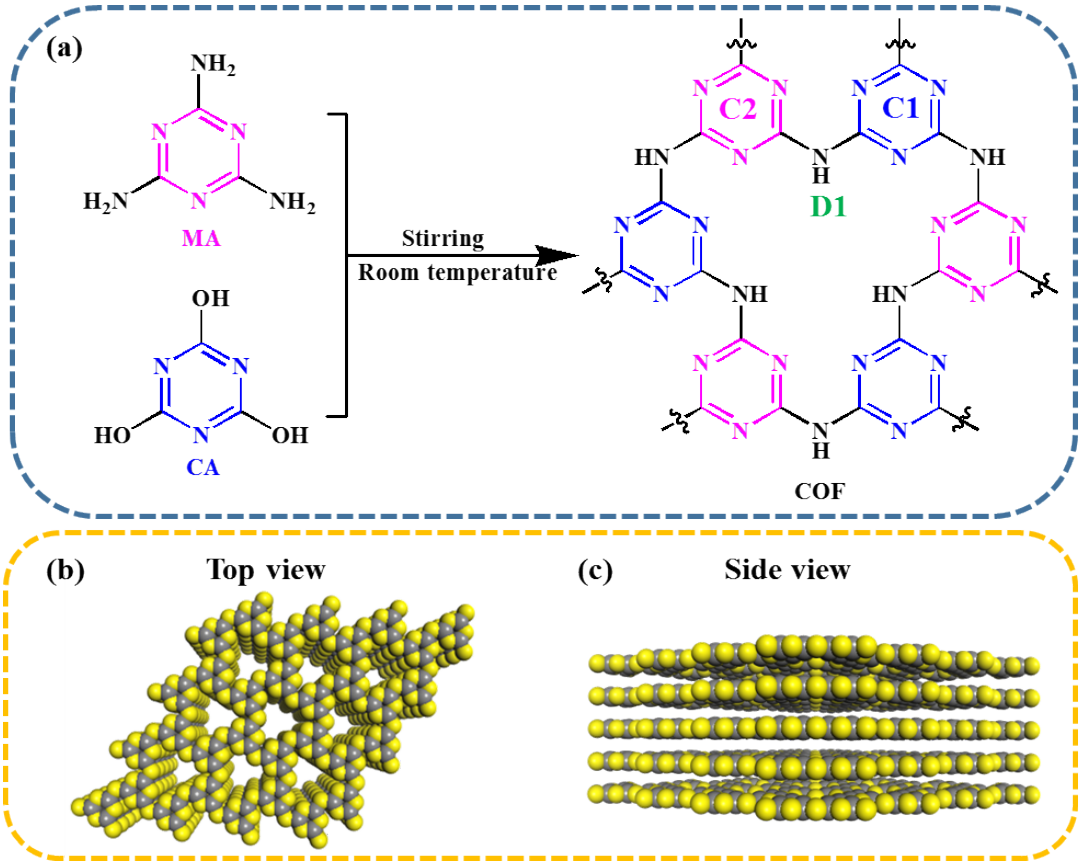

Figure S2 (**a**) Reaction mechanism. Topological structures of (**b**) top and (**c**) side view (H atoms are omitted for clarity.).

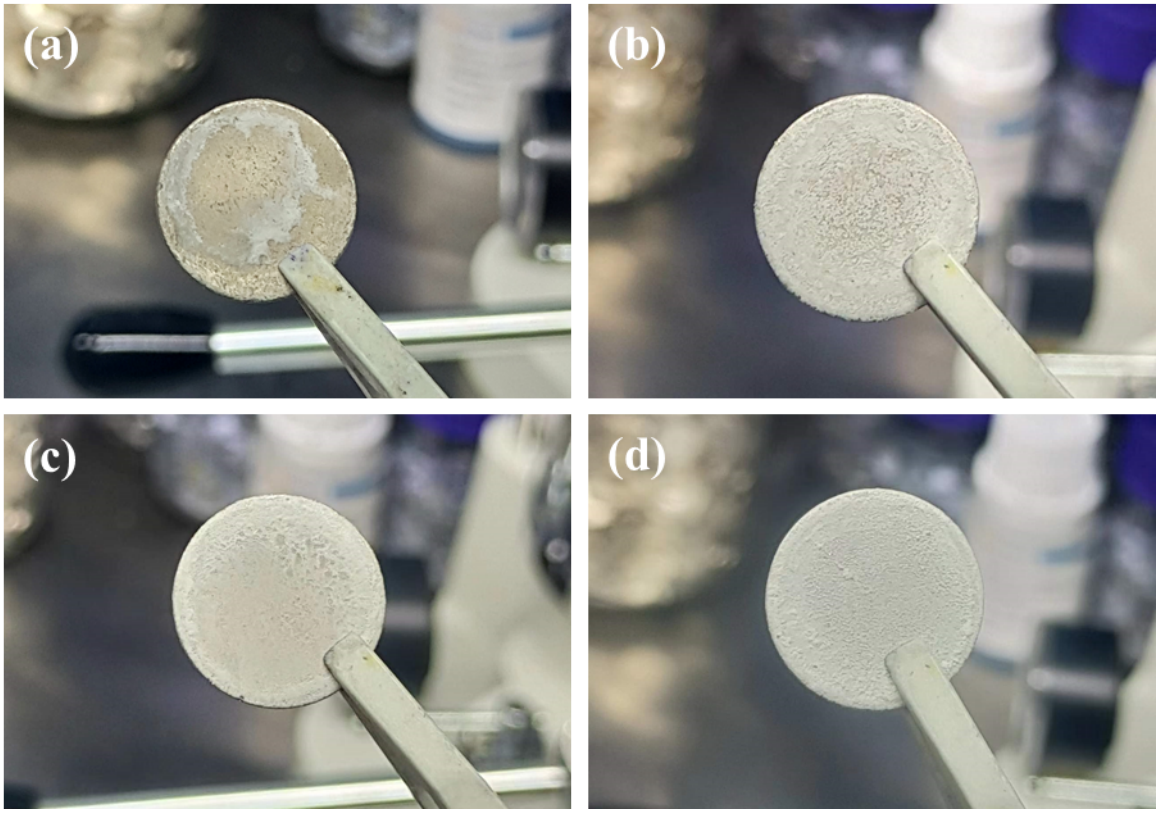

Figure S3 The COF@Li of (**a**) polished lithium foil without silanization treatment (10 μL CA solution); (**b-d**) the different mole (**b**: 5 μL, **c**: 8 μL, and **d**: 15 μL CA solution) COF grown on silanized Li foils.

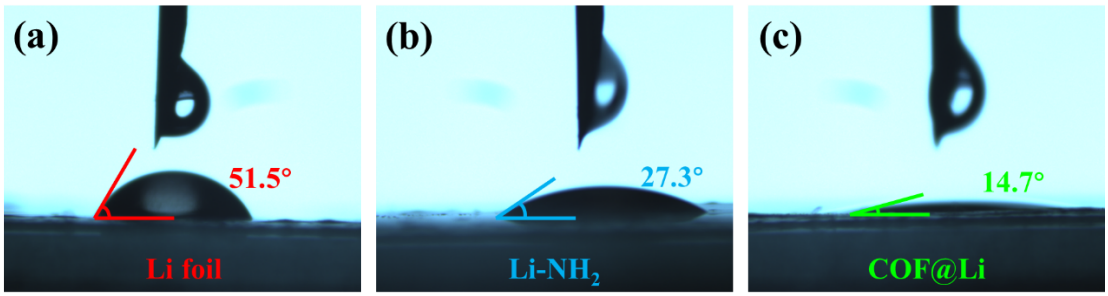

Figure S4 The contact angle test results of (**a**) Li foil (DMSO), (**b**) Li-NH_2 (DMSO), and (**c**) COF@Li (1.0 M LiTFSI dissolved in DOL and DME with 2 wt % $LiNO_3$).

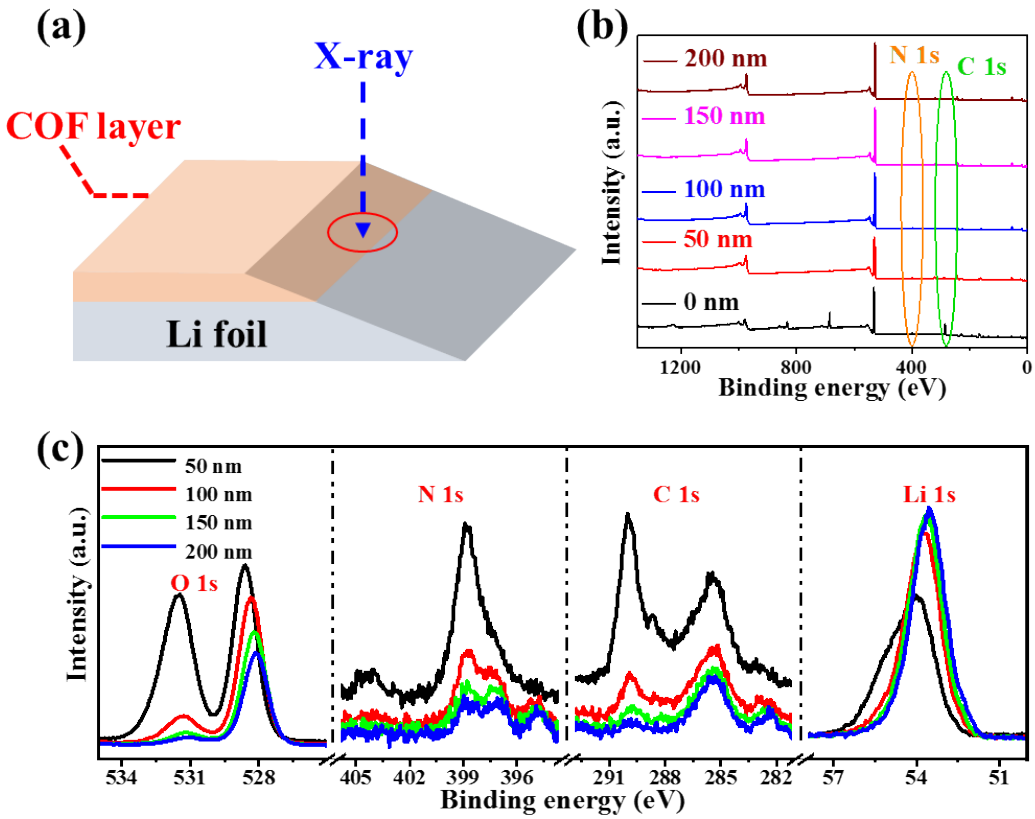

Figure S5 XPS depth profiles of the fresh COF@Li: (**a**) the model to be tested, (**b**) survey spectra and (**c**) high-resolution spectra of O 1s, N 1s, C 1s, and Li 1s peaks.

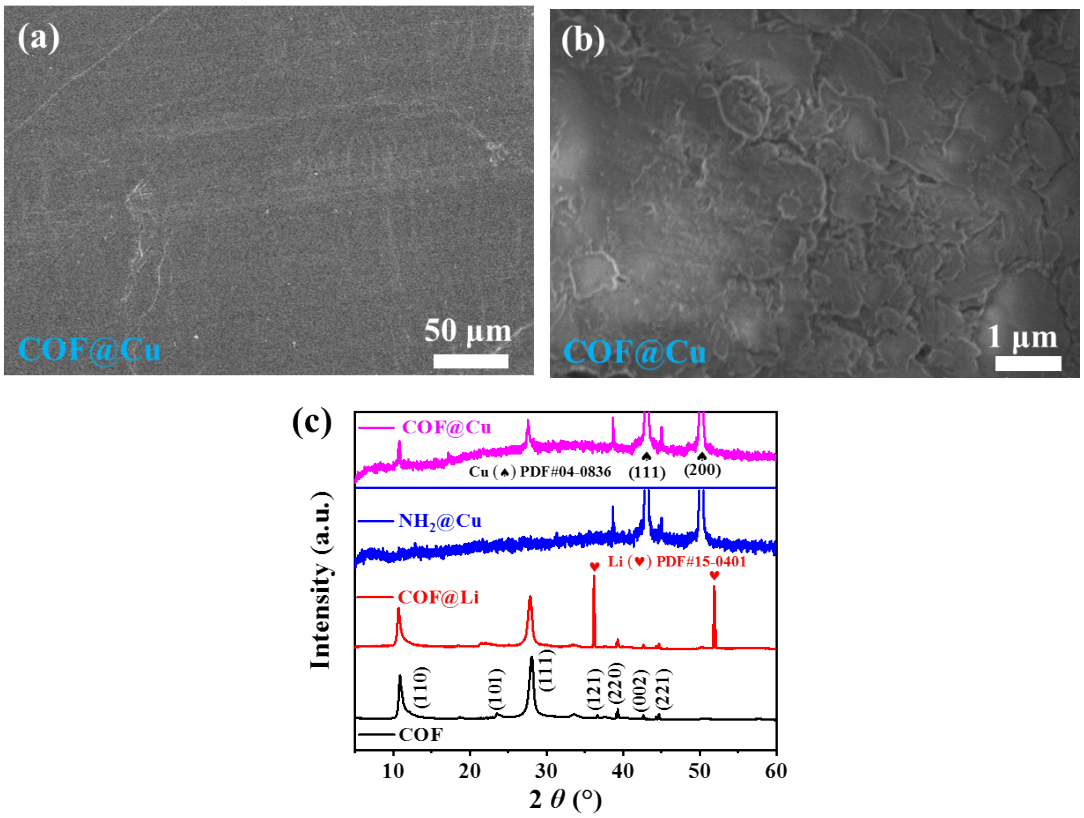

Figure S6. (**a-b**) Top-view morphology of COF@Cu for low and high resolution. (**c**) XRD patterns of COF, COF@Li, NH_2@Cu and COF@Cu.

The control COF@Cu sample was also synthesized by polymerization of COF on a Cu substrate under the same conditions as COF@Li. As shown in **Figure S6a** and **6b**, the surface morphology of COF@Cu revealed uniform distribution at both high and low resolution and this results are consistent with those obtained in Li foil. In terms of COF@Li, the characteristic diffraction peaks match well with the as-obtained COF (**Figure S6c**) and there are two strong characteristic diffraction peaks at 2θ = 31.2 and 52.0°, corresponding to the Li metal standard card (PDF#15-0401), indicating that the Li metal was not reacted with the generated H_2O. Besides, COF@Cu maintained the same characteristic diffraction peaks as those of COF in XRD, while NH_2@Cu only shows the characteristic diffraction peak of Cu substrate (2θ=43.1 and 50.2° correspond

to PDF#04-0836 of Cu), indicating that COF polymerization should have a reliable universality on inorganic substrates.

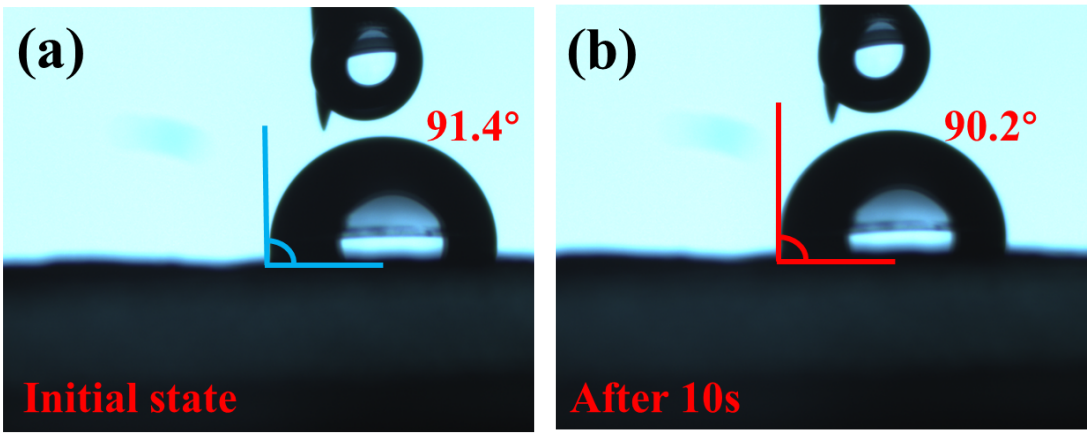

Figure S7 The contact angle for (**a**) the initial and (**b**) after 10 s of NH_2@Cu with H_2O.

The interface compatibility between the generated water and NH_2@Cu was analyzed. As shown in **Figure S7a**, the contact angle in the initial state reaches to 91.4°, indicating its good hydrophobicity. The contact angle remained at 90.2° after 10 s (**Figure S7b**), indicating that the silicified layer could not only form a polymerization point for COF growth, but also hinder the reaction of the generated water with lithium metal.

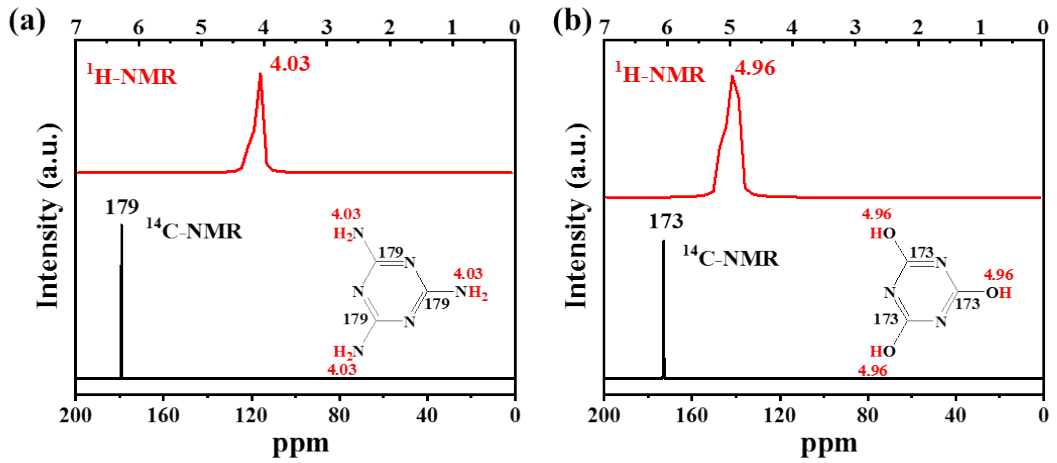

Figure S8 Solid-state ^{1}H-NMR and ^{14}C-NMR spectra of melamine and cyanuric acid.

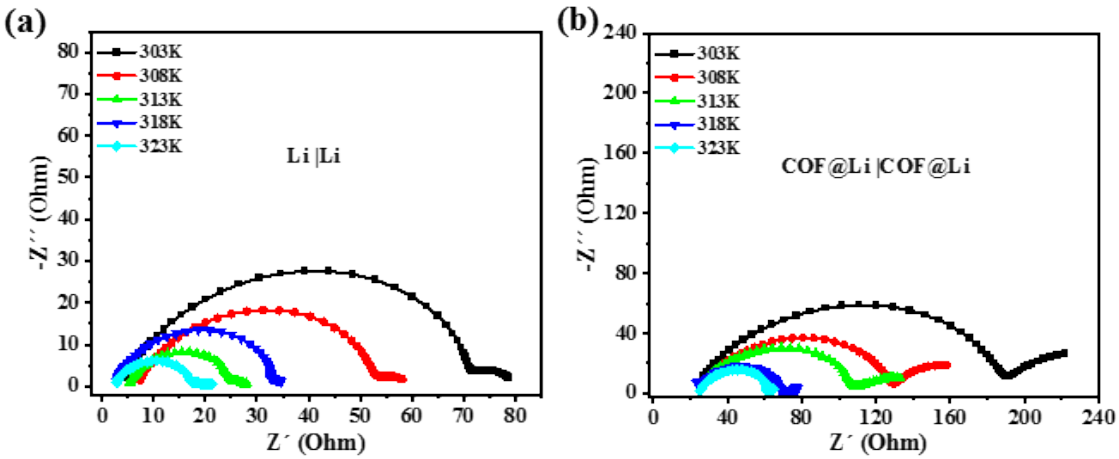

Figure S9 Nyquist plots of symmetric batteries with (**a**) and without (**b**) COF protection in the range of 303 to 323 K.

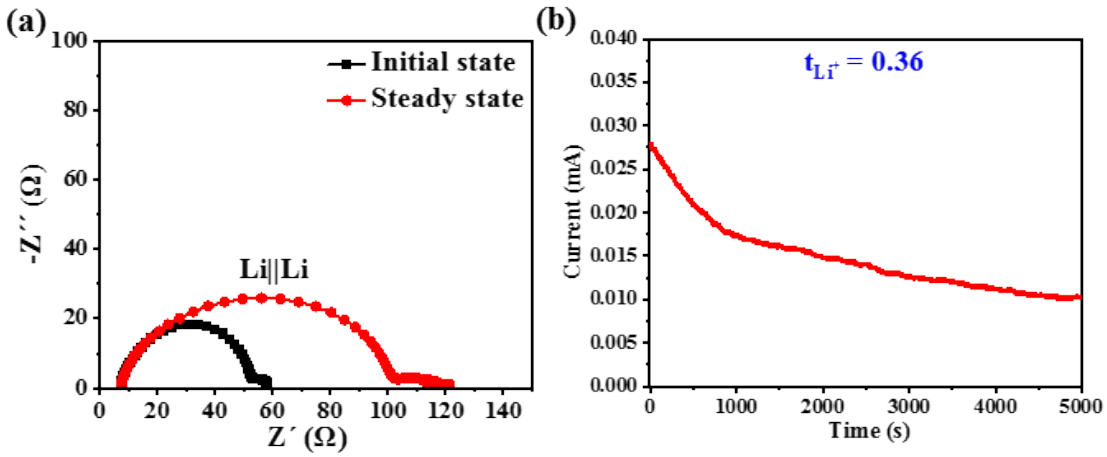

Figure S10 The Nyquist plots of impedance and Li ion transference number (t_{Li+}) of Li‖Li symmetric cells before and after polarization.

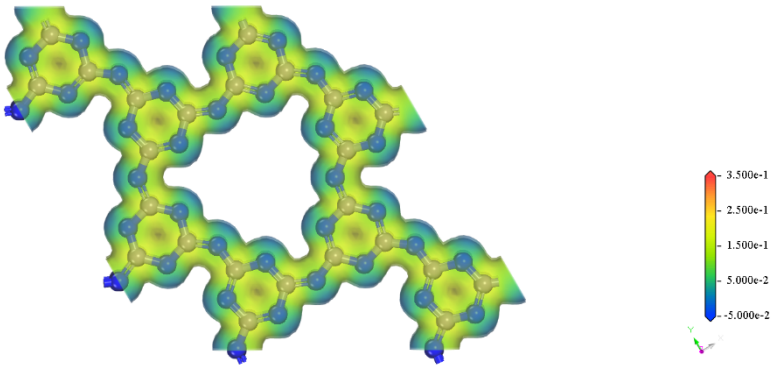

Figure S11 Simulation of the charge density differences of stacking COF interface.

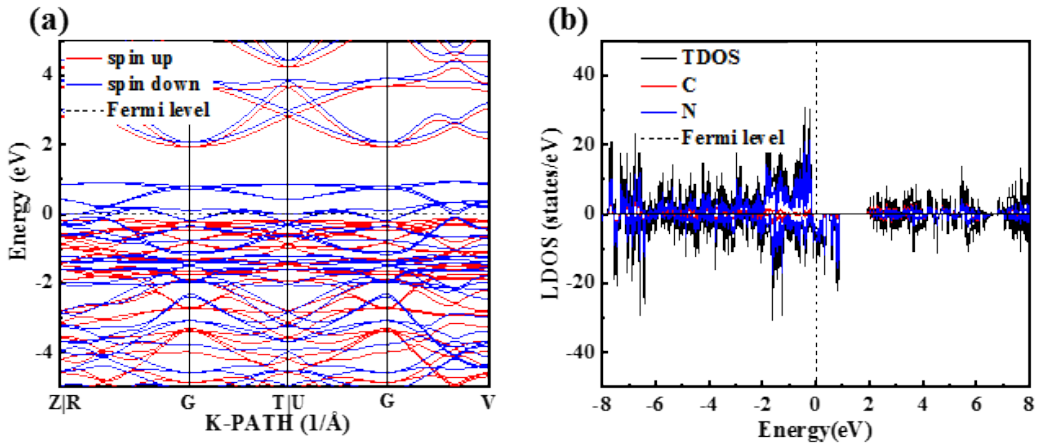

Figure S12 (**a**) Band structure and (**b**) local density of states of COF.

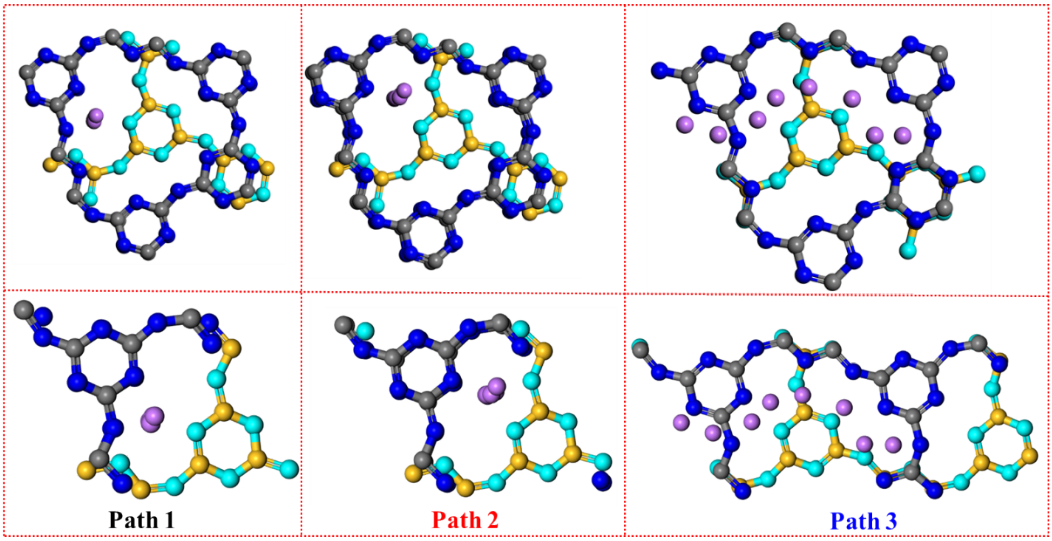

Figure S13 Top view of complete (top) and open schematic (bottom) for Li^+ diffusion pathways in COF topological structures.

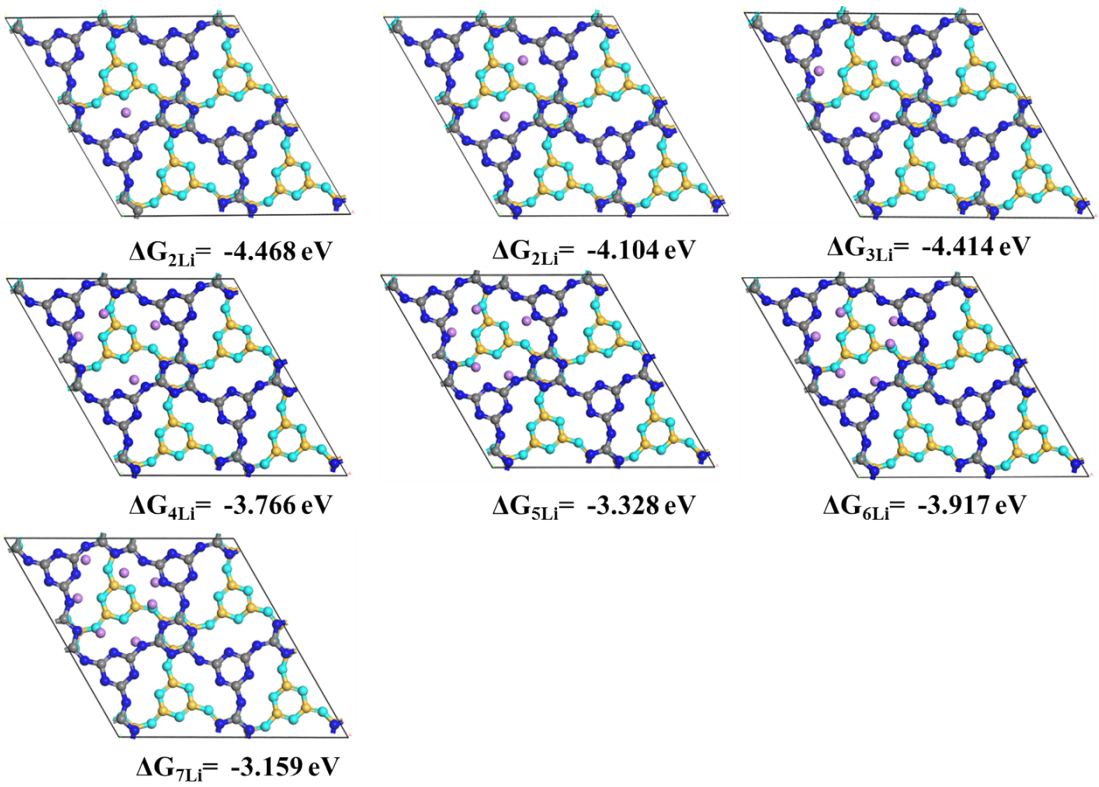

Figure S14 DFT simulation of Li plating and top view of Li atom adsorption on the most stable sites in COF topological structures.

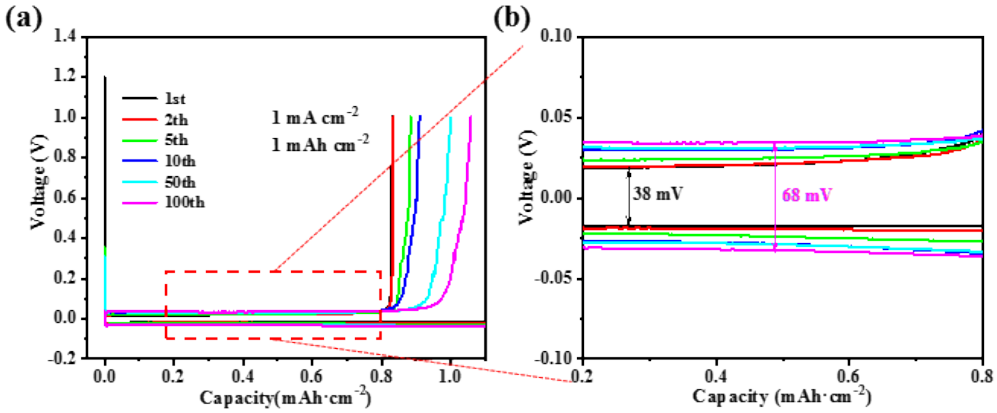

Figure S15 Voltage profiles of Li plating/stripping in symmetric cells with bare Li at 1 mA cm^{-2}/1 mAh cm^{-2}.

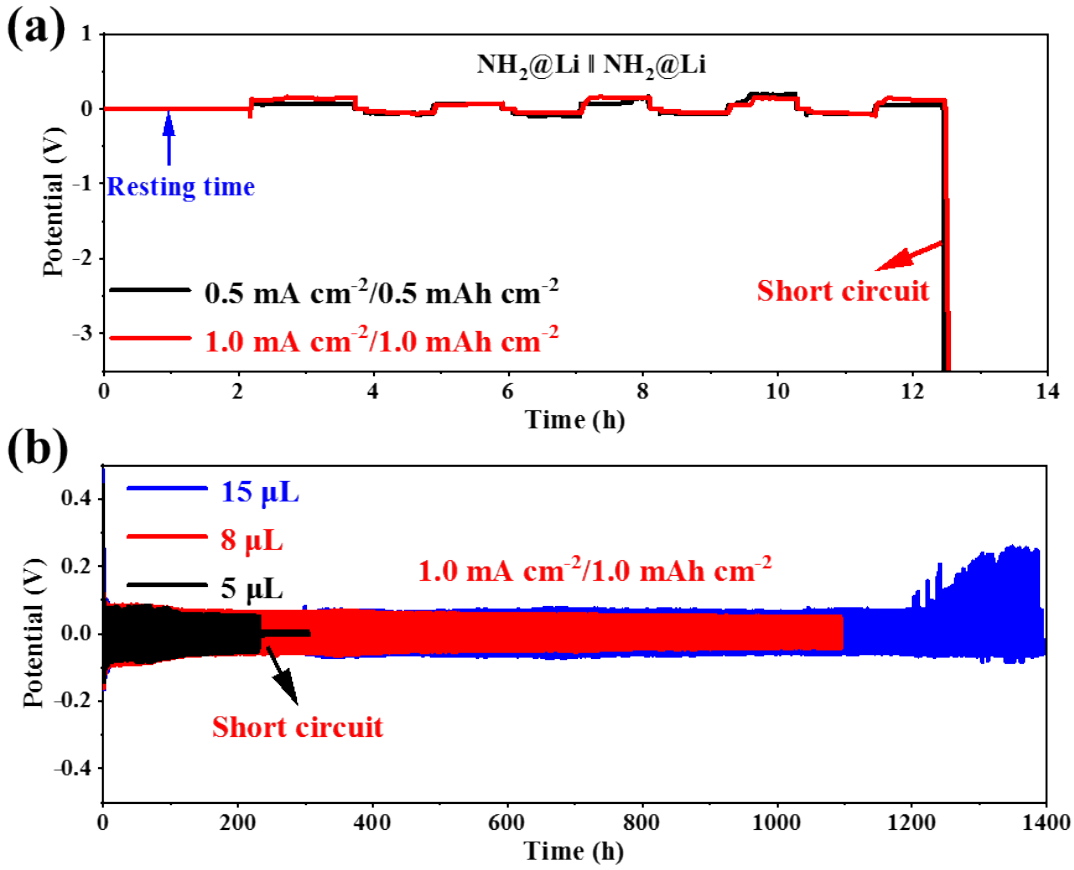

Figure S16 Cycling performance of symmetric cells for (**a**) NH_2@Li || NH_2@Li and (**b**) the different mole (5, 8 and 15 μL CA solution) COF grown on silanized Li foils.

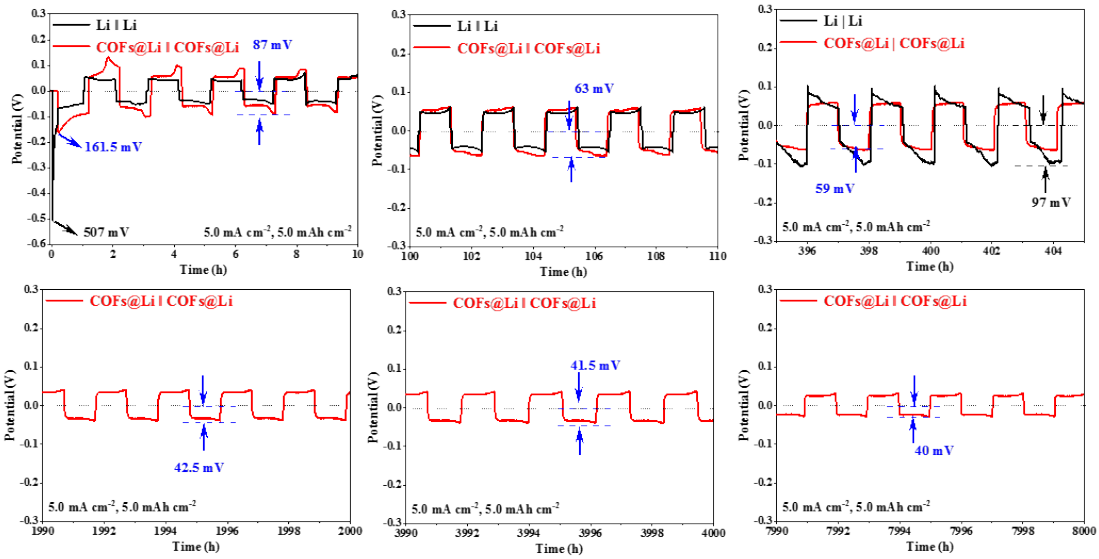

Figure S17 Voltage drop changes in different periods.

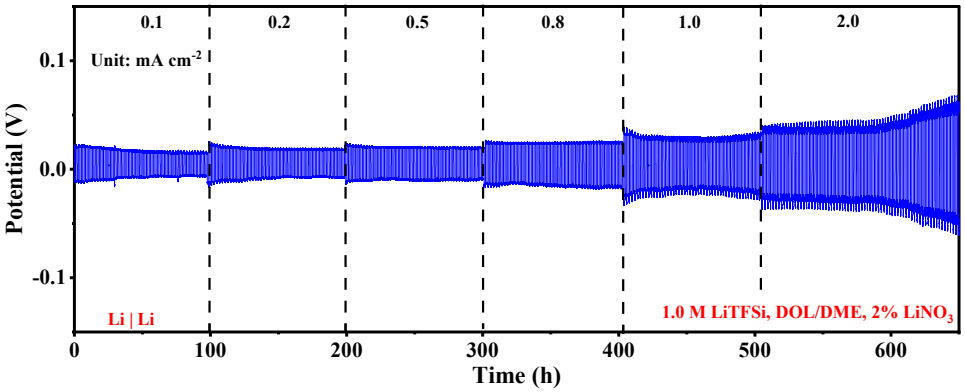

Figure S18 Rate performance of Li || Li symmetric cells with the current densities from 0.1 to 2.0 mA cm^{-2}.

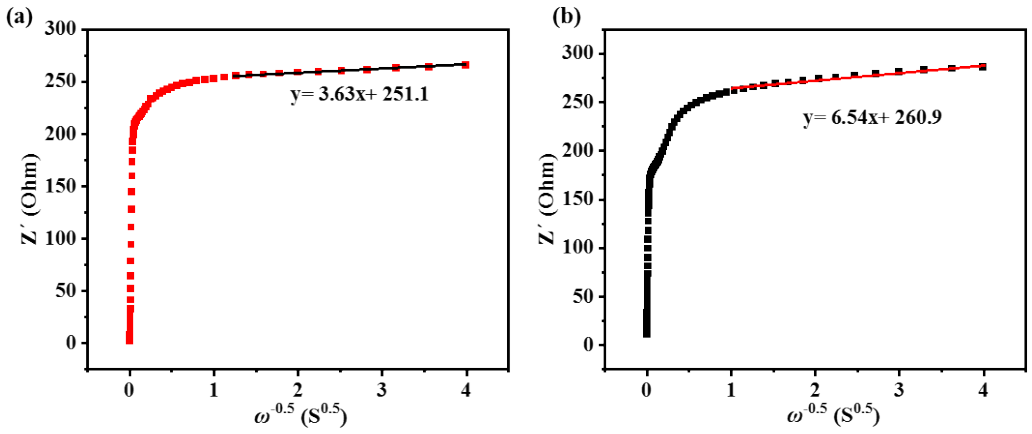

Figure S19 The relationship and fitted lines of Z' and frequency (ω) in (**a**) Li || Li and (**b**) COF@Li || COF@Li symmetric fresh cells.

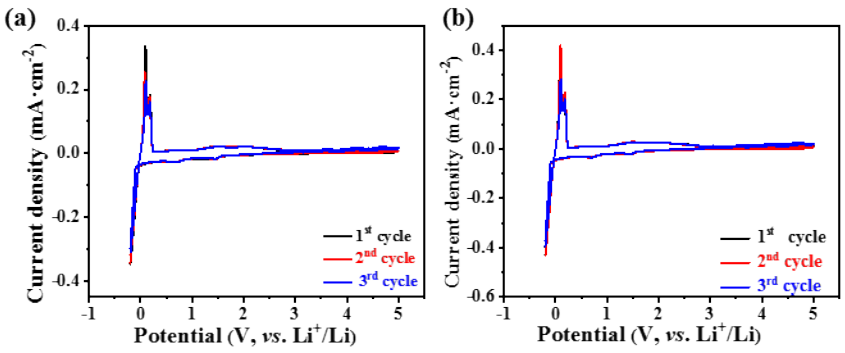

Figure S20 CV curves for the first 3 cycles of (**a**) Li| stainless cell and (**b**) COF@Li | stainless cell.

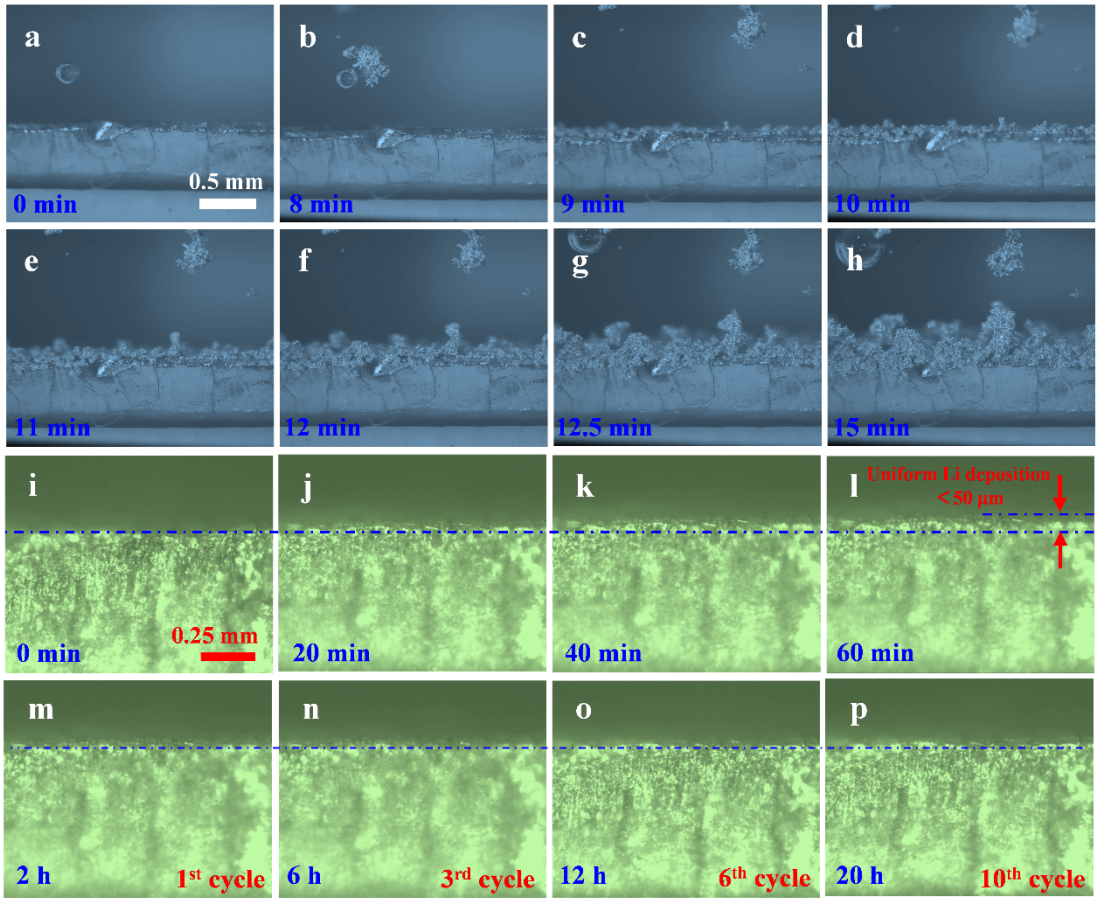

Figure S21 *In-situ* optical microscopy observations of the Li deposition process on (**a-h**) COF@Li and (**i-l**) COF@Li. (**m-p**) Morphologies of COF@Li after complete stripping in different cycles (the symmetric cell is firstly deposited (plated) the lithium metal for 1 hour and then stripped for 1 hour, that is one cycle).

For the Li || Li symmetric cell, the deposition processes were observed within 1 hour, and a large number of dendrites were generated. However, for the COF@Li || COF@Li symmetric cell, no obvious dendrite formation was monitored throughout the whole 10 cycles (20 h)).

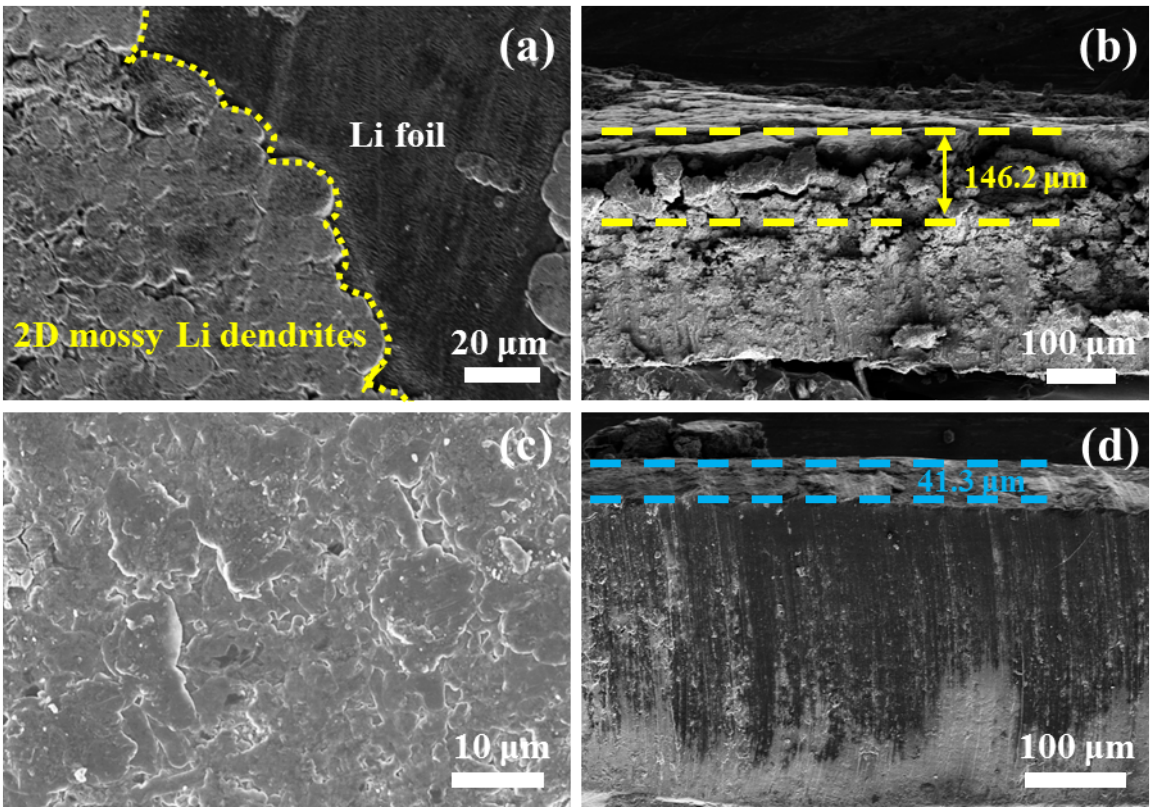

Figure S22 Top-view and cross-section SEM images of (**a-b**) Li foil after 100 cycles and (**c-d**) COF@Li after 1,000 cycles.

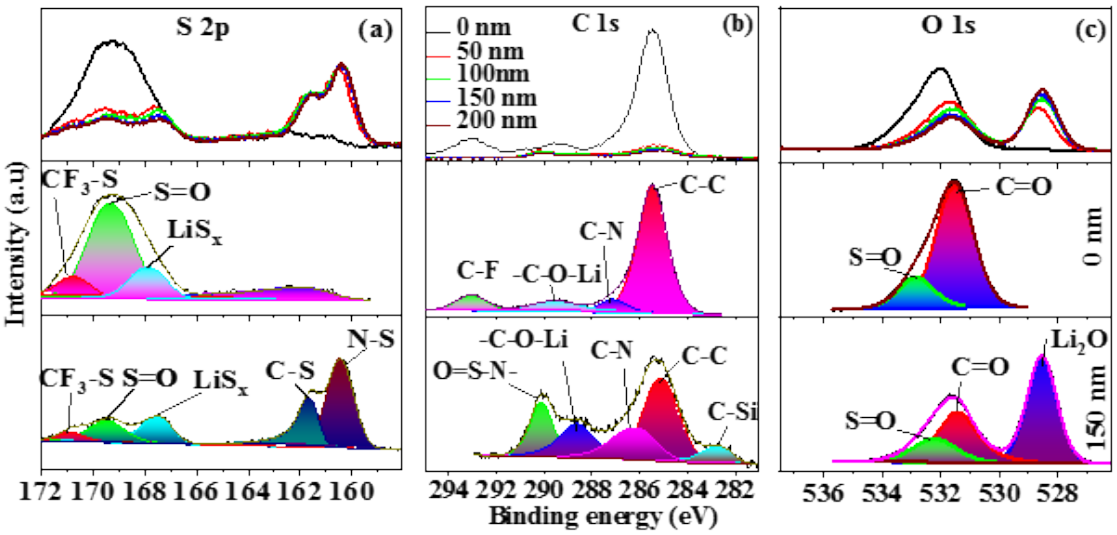

Figure S23 XPS spectra and high-resolution for COF@Li anodes after 1000 cycles:

(**a**) S 2p, (**b**) C 1s and (**c**) O 1s.

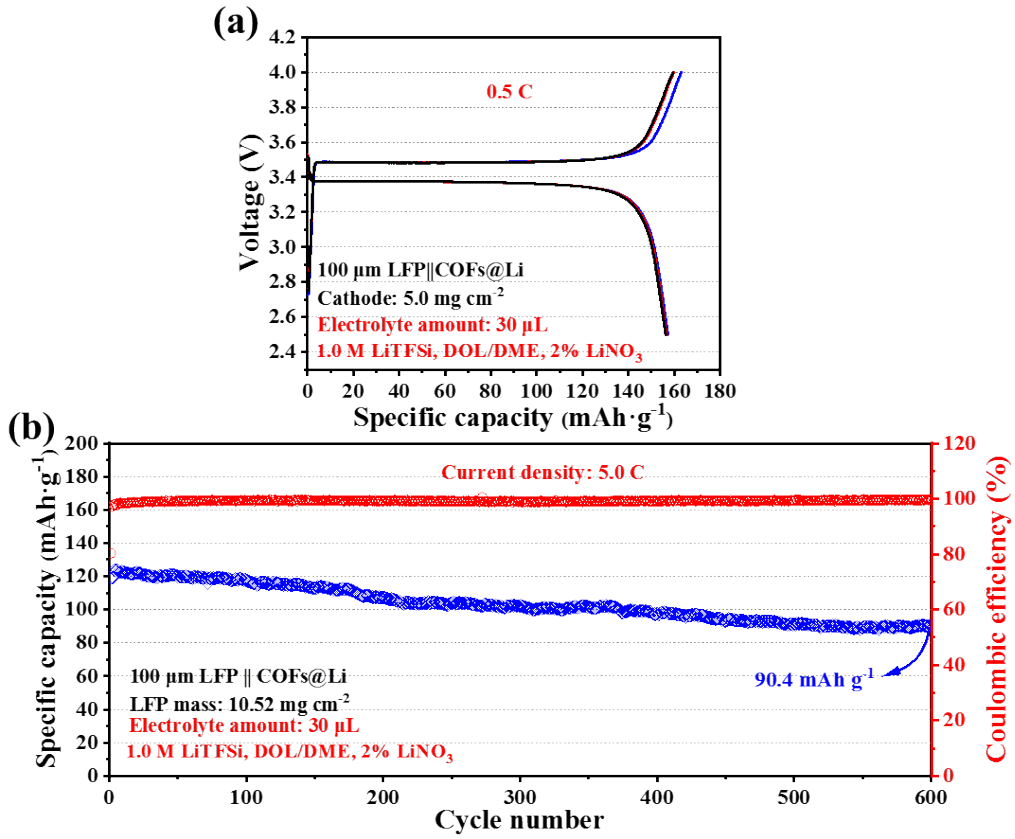

Figure S24 (**a**) The voltage profiles of LFP || COF@Li full cells for the first three cycles; (**b**) Cycling stability of LFP || COF@Li full cell with the LFP cathode of high mass loading (10.52 mg cm^{-2}).

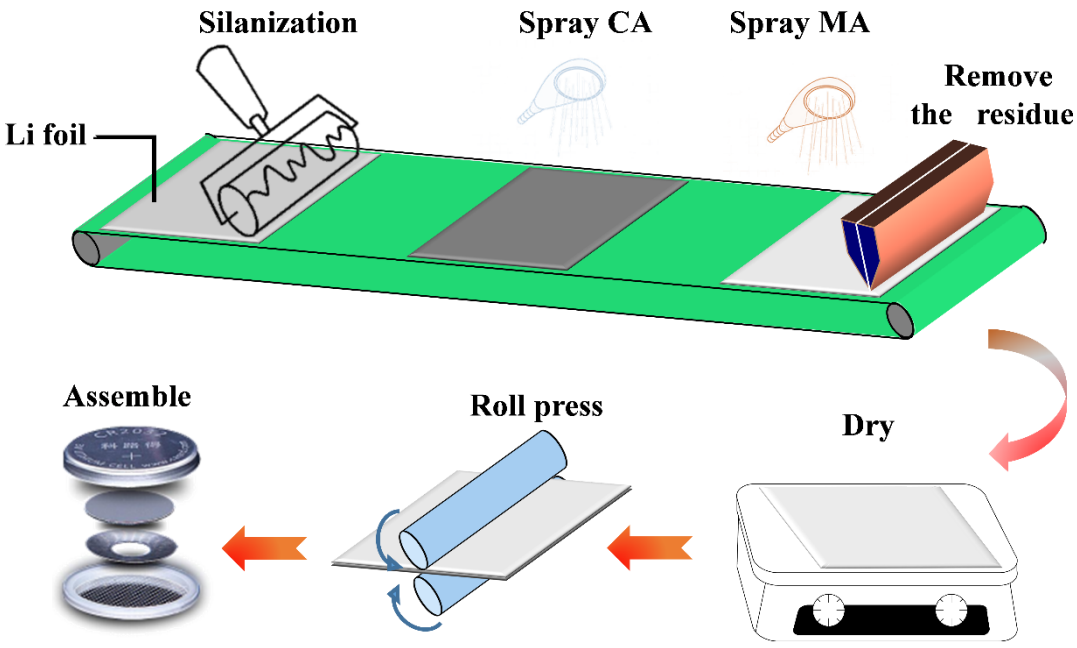

Figure S25 Schematic of the scale-up technology and practical fabrication process.

6. Tables

Table S1 The corresponding adsorption energy of COF obtained by DFT calculations.

Adsorption site	E_{total} **(eV)**	$E_{C2N3}\,(eV)$	E_{Li} **(eV)**	E_{ads} **(eV)**
Hole 1	**-977.63027**	**-970.92591**	**-0.2969018**	**-6.1374582**
Hole 2	**-976.76645**	**-970.54150**	**-0.29817149**	**-5.9267785**
N1	**-977.15039**	**-970.70820**	**-0.29799895**	**-6.14419105**
N2	**-977.08967**	**-970.65171**	**-0.29806911**	**-6.13989089**
C1	**-977.17638**	**-970.78929**	**-0.29814264**	**-6.08894736**
C2	**-977.33397**	**-970.83442**	**-0.29673457**	**-6.20281543**

Table S2 Cyclic stability comparison of our COF@Li anode with the previous reported modified SEI Li metal anode symmetric cells.

Modified	Current density (mA cm^{-2})	Area capacity (mAh cm^{-2})	Cycle time (h)	Refs.
DqTp@pp	4	1	600	[S6]
MA-Zn-C-Li	5	5	1500	[S7]
Zn-ZnO@PP	1	1	1200	[S8]
Li@PS40	1	1	400	[S9]
ACOF-Li	1	1	600	[S10]
[LiNBH]n	3	1	700	[S11]
Li_6PS5Cl-Li@Cu	1	1	500	[S12]
Li_3N by roll pressing	10	10	550	[S13]
Cu@CMC/SN	2	1	1500	[S14]
Li@LiF	1	1	630	[S15]
PCNF/MoS_2-Li,	1	1	750	[S16]
Li/G@PVDF-HFP	0.5	1	2200	[S17]
OPHS-Li	10	5	2500	[S18]
Li/$CoSe_2$@NC	1	1	1000	[S19]
SPF/Li	5	1	3400	[S20]
ICE-Li	20	20	500	[S21]
Li/graphene-C/Li_3N	1	1	1000	[S22]
NCL-Li	1	3	1000	[S23]

NFF@Li	2	0.5	1000	[S24]
CF@Cu_2O NWAs@PDA	3	1	1000	[S25]
COF@Li	**5**	**5**	**8000**	**This**
	20	**20**	**1600**	**work**

Table S3 Equivalent impedance fitting parameters by the Zview software for 1st and 200th cycles.

Sample	COF@Li || COF@Li		Li || Li	
	1st cycle	**200th cycles**	**1st cycle**	**200th cycles**
R_s (Ω)	7.47	7.46	7.33	7.31
R_{ct} (Ω)	169.9	161.64	213.3	394.59
R_{SEI} (Ω)	65.2	32.65	22.08	28.89
W (Ω)	52.87	57.36	26.41	121.2
CPE1 (Ω)	30.85	243.3	19.28	72.09
CPE2 (Ω)	41.48	157.9	7.82	56.23

References

[S1] G. Kresse and J. Furthmüller, *Comp. Mater. Sci.*, 1996, **6**, 15-50.

[S2] P. E. Blöchl, Projector augmented-wave method, *Phys Rev B*: *Condens Matter.*, 1994, **50**, 17953-17979.

[S3] J. P. Perdew, J. A. Chevary, S. H. Vosko, Koblar A. Jackson, M. R. Pederson, D. J. Singh and C. Fiolhais, *Phys. Rev. B*, 1992, **46**, 6671-6687.

[S4] S. Grimme, J. Antony, S. Ehrlich and H. Krieg, *J. Chem. Phys.*, 2010, **132**, 154104.

[S5] G. Henkelman, B. P. Uberuaga and H, Jónsson, *J. Chem. Phys.*, 2000, **113**, 9901-9904.

[S6] Z. Li, W. Y. Ji, T.-X. Wang, X. S. Ding, and B.-H. Han, *Chem. Eng. J.*, 2022, **437**, 135293.

[S7] F. Wang, J. X. Gao, Y. Liu, F. Z. Ren, *J. Mater. Chem. A*, 2022, **10**, 17395-17405.

[S8] L. Lin, F. Liu, Y. G. Zhang, C. Z. Ke, H. F. Zheng, F. J. Ye, X. L. Yan, J. Lin, B. S. Sa, L. S. Wang, D.-L. Peng, and Q. S. Xie, *ACS Nano*, 2022, **16**, 13101-13110.

[S9] G. Song, C. Hwang, W.-J. Song, J. H. Lee, S. Lee, D.-Y. Han, J. Kim, H. Park, H.-K. Song and S. Park, *Small*, 2022, **18**, 2105724.

[S10] X. Li, Y. Tian, L. Shen, Z. B. Qu, T. Q. Ma, F. Sun, X.Y. Liu, C. Zhang, J. Q. Shen, X. Y. Li, L. N. Gao, S. X. Xiao, T. F. Liu, Y. Liu and Y. F. Lu, *Adv. Funct. Mater.*, 2021, **31**, 2009718.

[S11] Z. Wang, Y. Y. Wang, Z. H. Zhang, X. W. Chen, W. Lie, Y.-B. He, Z. Zhou, G. L. Xia and Z. P. Guo, *Adv. Funct. Mater.*, 2020, **30**, 2002414.

[S12] Y. Ye, Y. Y. Zhao, T. Zhao, S. N. Xu, Z. X. Xu, J. Qian, L. L. Wang, Y. Xing,

L. Wei, Y. J. Li, J. L. Wang, L. Li, F. Wu and R. J. Chen, *Adv. Mater.*, 2021, **33**, 2105029.

[S13] C. Chen, Q. W. Liang, G. Wang, D. D. Liu and X. H. Xiong, *Adv. Funct. Mater.*, 2022, **32**, 2107249.

[S14] T.-T. Su, J.-B. Le, W.-F. Ren, S.-J. Zhang, J.-M. Yuan, K. Wang, C.-Y. Shao, J.-T. Li, S.-G. Sun, and R.-C. Sun, *J. Power Sources*, 2022, **521**, 230949.

[S15] S. Liu, S. S. Liu, Y. L. Ma, J. J. Wang, P. J. Zuo, C. Y. Du, G. P. Yin and Y. Z. Gao, *Chem. Eng. J.*, 2022, **427**, 131625.

[S16] L. Yu, L. T. Yu, Q. M. Su, B. Y. Li, L. Huang, G. H. Du, S. K. Ding, W. Q. Zhao, M. Zhang and B. S. Xu, *Chem. Eng. J.*, 2022, **429**, 132479.

[S17] Z. Liu, B. Y. He, Z. B. Zhang, W. Deng, D. J. Dong, S. J. Xia, X. F. Zhou and Z. P. Liu, *ACS Appl. Mater. Interf.*, 2022, **14**, 2871-2880.

[S18] Q. Wang, J. Wan, X. Cao, R. Wen, Y. G. Guo, W. Liu and H. H. Zhou, *Adv. Funct. Mater.*, 2022, **32**, 2107923.

[S19] J. Xu, L. L. Xu, Z.L. Zhang, B. Sun, Y. Jin, Q. Z. Jin, H. Liu and G. X. Wang, *Energy Storage Mater.*, 2022, **47,** 223-234.

[S20] Z. Ju, G. X. Lu, O. W. Sheng, H. D. Yuan, , S. Q. Zhou, T. F. Liu, Y. J. Liu, Y. Wang, J. W. Nai, W. K. Zhang and X. Y. Tao, *Nano Lett.*, 2022, **22**, 1374-1381.

[S21] K. Li, Z. L. Zhu, R. R. Zhao, H. R. Du, X. Q. Qi, X. B. Xu and L. Qie, *Energy Environ. Mater.*, 2022, **5**, 337-343.

[S22] M. T. Wan, X. R. Duan, H. Cui, J. M. Du, L. Fu, Z. H. Chen, Z. Lu, G. C. Li, Y. J. Li, E. Y. Mao, L. Wang and Y. M. Sun, *Energy Storage Mater.*, 2022, **46**, 563-569.

[S23] H. Liu, R. M. Tao, C. Guo, W. Zhang, X. L. Liu, P. M. Guo, T. Y. Zhang and J. Y. Liang, *Chem. Eng. J.*, 2022, **429**, 132239.

[S24] W. Hou, S. B. Li, J. X. Liang, B. Yuan, R. Z. Hu, *Electrochim. Acta*, 2022, **402**, 139561.

[S25] X.-F. Liu, D. Xie, F.-Y. Tao, W.-Y. Diao, J.-L. Yang, X.-X. Luo, W.-L. Li and X.-L. Wu, *ACS Appl. Mater. Interfaces*, 2022, **14**, 23588-23596.